

End-To-End Deep Learning-based Adaptation Control for Linear Acoustic Echo Cancellation

Thomas Haubner, *Student Member, IEEE*, Andreas Brendel, *Member, IEEE*,
and Walter Kellermann, *Life Fellow, IEEE*

Abstract—The attenuation of acoustic loudspeaker echoes remains to be one of the open challenges to achieve pleasant full-duplex hands free speech communication. In many modern signal enhancement interfaces, this problem is addressed by a linear acoustic echo canceler which subtracts a loudspeaker echo estimate from the recorded microphone signal. To obtain precise echo estimates, the parameters of the echo canceler, i.e., the filter coefficients, need to be estimated quickly and precisely from the observed loudspeaker and microphone signals. For this a sophisticated adaptation control is required to deal with high-power double-talk and rapidly track time-varying acoustic environments which are often faced with portable devices. In this paper, we address this problem by end-to-end deep learning. In particular, we suggest to infer the step-size for a least mean squares frequency-domain adaptive filter update by a Deep Neural Network (DNN). Two different step-size inference approaches are investigated. On the one hand broadband approaches, which use a single DNN to jointly infer step-sizes for all frequency bands, and on the other hand narrowband methods, which exploit individual DNNs per frequency band. The discussion of benefits and disadvantages of both approaches leads to a novel hybrid approach which shows improved echo cancellation while requiring only small DNN architectures. Furthermore, we investigate the effect of different loss functions, signal feature vectors, and DNN output layer architectures on the echo cancellation performance from which we obtain valuable insights into the general design and functionality of DNN-based adaptation control algorithms.

Index Terms—Acoustic echo cancellation, system identification, adaptation control, step-size control, double-talk detection, DNN

I. INTRODUCTION

The attenuation of loudspeaker echoes is a crucial component of any full-duplex hands-free speech communication interface [1]. In general, there are two main algorithmic approaches to achieve this goal: Acoustic Echo Cancellation (AEC) and Acoustic Echo Suppression (AES) [1]. While echo cancelers attenuate the unwanted signal components by subtracting a loudspeaker echo estimate from the microphone signal, echo suppressors directly filter the microphone signal with a postfilter [1]. In many modern speech enhancement algorithms, both approaches are combined by applying a post-filter to the echo-reduced error signal of the echo canceler [1],

[2]. Despite recent progress by deep learning-based postfilters, the benefit of additionally using an echo canceler is significant [3]–[5]. Yet, the full potential of an echo canceler is only obtained, if its model parameters are precisely inferred from the observed loudspeaker and microphone signals. For this, the continuous minimization of the microphone error signal power by gradient descent-based parameter updates has proven to be a powerful tool [6]. Yet, a sophisticated adaptation, i.e., step-size, control is required to rapidly track time-varying acoustic scenes and deal with high-power double-talk and noise [7].

Adaptation control has evolved in the last decades from simple binary stall-or-adapt methods [8], [9], which mainly considered double-talk, to advanced continuous step-size estimators which employ complex probabilistic models [10]–[17]. In particular, the inference of the model parameters by Kalman filtering [11], [12] or semi-supervised blind source separation [15]–[17] can be considered as state of the art according to recent challenge results [3]–[5]. Yet, the performance of these traditional step-size estimators relies on the precise estimation of statistics of unobserved signals, e.g., the near-end speech and noise Power Spectral Densities (PSDs), which are difficult to obtain in practice [18]. Traditional estimators of these quantities often suffer from sensitive hyperparameter choices which do not generalize well to different acoustic scenes [18]. To remedy this limitation, it has recently been proposed to use machine learning models to support traditional step-size estimators [19], [20]. In particular, the approximation of the interference PSD of the Kalman filter model, capturing near-end speech and noise, by non-negative dictionaries [19] and Deep Neural Networks (DNNs) [20] has shown significant performance improvements relative to traditional, i.e., non-trainable, PSD estimators. Besides the support of traditional step-size estimators by trainable PSD models, machine learning has also been used to directly approximate optimum step-sizes of a time-domain Normalized Least-Mean-Squares (NLMS) algorithm [21] or Short-Time Fourier Transform (STFT)-domain recursive least squares algorithm [22]. Yet, despite significant performance improvements, it remains unclear whether machine learning-supported approximation of target step-sizes, e.g., a Kalman filter step-size with oracle statistics, is optimum w.r.t. echo cancellation performance. Furthermore, the loss function design for training the machine learning models is challenging, as the effect of PSD or step-size estimation errors on the AEC performance is complicated. Therefore, it has recently been proposed to optimize DNN-based step-size estimators directly w.r.t. the echo estimation quality which is typically termed end-to-end training [23]–[29]. The various

This article has been submitted to *IEEE/ACM Transactions on Audio, Speech, and Language Processing*.

Thomas Haubner and Walter Kellermann are with the chair of Multimedia Communications and Signal Processing (LMS), Friedrich-Alexander-Universität Erlangen-Nürnberg, D-91058 Erlangen, Germany. Andreas Brendel contributed to the work while he was at LMS. He is now with the Fraunhofer Institute for Integrated Circuits (IIS), D-91058 Erlangen, Germany. e-mail: {thomas.haubner;andreas.brendel;walter.kellermann}@fau.de
Digital Object Identifier

approaches differ in the echo estimation model, feature design, DNN integration and loss function design. While [23], [25]–[27] employ a time-domain Finite Impulse Response (FIR) echo estimation model which is optimized in the frequency domain, [24], [26], [28], [29] consider a Convolutional Transfer Function (CTF) model (cf. e.g. [30]–[32]) which operates in the STFT domain. Furthermore, while [23], [25]–[27] investigate linear echo estimation models, [24], [28], [29] consider additionally non-linear pre-processors to deal with hardware imperfections, e.g., loudspeaker distortions. Another key difference is given by the integration of the DNN into the filter update. In [26]–[28], it is proposed to directly estimate the gradient, or parts of it, by complex-valued DNNs. In contrast, [23]–[25], [29] propose to infer only parameters of traditional step-size estimators while keeping the gradient direction of the respective filter update unchanged. Furthermore, various step-size inference architectures have been considered ranging from broadband approaches, which jointly estimate a frequency-selective step-size vector with a single DNN, [23]–[25], to narrowband approaches, which use individual DNNs per frequency band [26], [28], [29]. In addition, joint control of frequency groups has been investigated [27]. Finally, there are also echo cancellation algorithms which exploit no physical knowledge for designing the echo estimation model but instead use a completely data-driven DNN-based estimator [33]–[35].

In this paper, we provide a general view on deep learning-based adaptation control for linear AEC and the differences between broadband and narrowband step-size inference architectures. By investigating their benefits and disadvantages, we introduce a new hybrid control strategy which combines the low DNN parameter count of narrowband step-size estimators with the capability of broadband approaches to exploit information from the entire frequency spectrum. All three generic adaptation control approaches, i.e., narrowband, broadband, and hybrid, are compared for a variety of challenging AEC scenarios. Furthermore, we analyze the effect of different features, loss functions and DNN output layer designs on the echo cancellation performance. As a specific parameterization of our adaptation control algorithm is equivalent to a basic DNN-based control of the NLMS algorithm, the conclusions are broadly applicable. Additionally, to gain deeper insights into the DNN-based step-size estimator, we analyze its internal states and step-size estimates by comparing them to the spectrograms of the individual microphone signal components. Finally, we provide the code for training the DNNs¹ to simplify future comparison of different DNN-based adaptation control algorithms and fuel the research on further developments.

The remainder of the paper is structured as follows: In Sec. II, we define a signal model which describes a generic hands-free speech communication interface. Subsequently, the proposed deep learning-based adaptation control algorithms are introduced in Sec. III and their relation to traditional approaches is discussed. An experimental evaluation follows in Sec. IV and conclusions are presented in Sec. V.

In the following, we use f and τ as frequency and frame index of STFT-domain quantities, respectively. The corre-

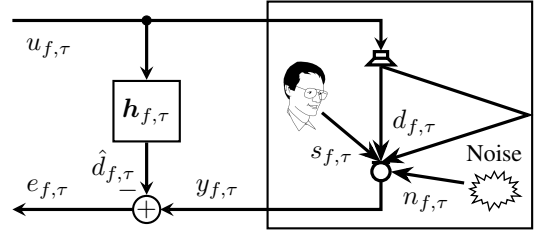


Fig. 1: Block diagram of a linear acoustic echo canceler operating in the frequency domain.

sponding time-domain signals are denoted by an underline and κ is used as the sample index. The real and imaginary components of a complex-valued number $z \in \mathbb{C}$ are denoted by $\mathcal{R}\{z\}$ and $\mathcal{I}\{z\}$, respectively, and its complex conjugate by z^* . The Euclidean norm of a vector is denoted by $\|\cdot\|$ and its transpose by $(\cdot)^T$. Additionally, we introduce the all-one vector $\mathbf{1}_F$ of dimension F and the expectation operator $\mathbb{E}[\cdot]$. Finally, the l th diagonal element of a matrix is written as $[\cdot]_{ll}$.

II. LINEAR ACOUSTIC ECHO CANCELLATION

This section introduces the signal model and the filter update which are commonly used for linear acoustic echo cancelers operating in the frequency domain as shown in Fig. 1.

A. Signal Model

We model the STFT-domain microphone signal $y_{f,\tau}$ as a linear superposition of an echo component $d_{f,\tau}$, a near-end speech component $s_{f,\tau}$ and a background noise component $n_{f,\tau}$ as follows:

$$y_{f,\tau} = d_{f,\tau} + s_{f,\tau} + n_{f,\tau} \in \mathbb{C}. \quad (1)$$

The goal of AEC is to obtain a precise echo estimate $\hat{d}_{f,\tau}$ which is subtracted from the microphone signal $y_{f,\tau}$ to obtain an ideally echo-free error signal

$$e_{f,\tau} = y_{f,\tau} - \hat{d}_{f,\tau} \quad (2)$$

as shown in Fig. 1. In the following, we assume the popular CTF echo estimation model [30]–[32] which suggests a linear FIR filter model in each frequency band

$$\hat{d}_{f,\tau} = \mathbf{h}_{f,\tau-1}^T \mathbf{u}_{f,\tau} \quad (3)$$

with the length- L filter coefficient vector

$$\mathbf{h}_{f,\tau-1}^T = (h_{0,f,\tau-1} \quad \dots \quad h_{L-1,f,\tau-1}) \quad (4)$$

and the STFT-domain loudspeaker signal vector

$$\mathbf{u}_{f,\tau}^T = (u_{f,\tau} \quad \dots \quad u_{f,\tau-L+1}). \quad (5)$$

B. Adaptive Filter Estimation

The filter coefficient vector $\mathbf{h}_{f,\tau-1}$ should ideally be updated such that the residual echo power $\mathbb{E}[|d_{f,\tau} - \hat{d}_{f,\tau}|^2]$ is minimized. Yet, as the echo statistics are not known in practice,

¹https://github.com/ThomasHaubner/e2e_dnn_ad_control_for_lin_aec

filter coefficient updates are typically derived by iteratively minimizing the microphone error signal power²

$$\psi_{f,\tau}^{\text{EE}} = \mathbb{E} \left[|e_{f,\tau}|^2 \right] = \mathbb{E} \left[\left| d_{f,\tau} - \hat{d}_{f,\tau} + z_{f,\tau} \right|^2 \right] \quad (6)$$

with $z_{f,\tau} = s_{f,\tau} + n_{f,\tau}$ denoting the interference component w.r.t. the filter estimation task. Note that the interference $z_{f,\tau}$ includes also all echo components which cannot be described by the linear CTF model (3), e.g., echoes resulting from late reverberation or loudspeaker non-linearities. The most popular filter optimization method is given by the LMS update [6]

$$h_{l,f,\tau} = h_{l,f,\tau-1} + \mu_{l,f,\tau} (u_{f,\tau-l}^* e_{f,\tau}) \quad (7)$$

with $\mu_{l,f,\tau} \geq 0$ being a tap-, frequency- and time-dependent step-size. Yet, by assuming the residual echo signal $d_{f,\tau} - \hat{d}_{f,\tau}$ and the interference component $z_{f,\tau}$ to be orthogonal, we easily conclude from (6) that the error signal power $\mathbb{E}[|e_{f,\tau}|^2]$ is only a good approximation of the residual echo power $\mathbb{E}[|d_{f,\tau} - \hat{d}_{f,\tau}|^2]$ for time-frequency bins with a high Echo-to-Interference Power Ratio (EIR)

$$\text{EIR}_{f,\tau} = 10 \log_{10} \frac{\mathbb{E} \left[|d_{f,\tau}|^2 \right]}{\mathbb{E} \left[|z_{f,\tau}|^2 \right]}. \quad (8)$$

To remedy this limitation the step-size $\mu_{l,f,\tau}$ in the LMS update (7) must be adapted to the respective signal statistics as will be discussed in the following.

III. ADAPTATION CONTROL

In this section, we introduce and motivate the general concept of deep learning-based step-size estimation and discuss different generic variants.

A. Traditional Approaches

We first introduce traditional model-based methods which will serve as a basis for the deep learning-based approaches described in the sequel. The majority of these methods suggests a mapping of certain signal expectations, e.g., the loudspeaker and interference powers $\psi_{f,\tau}^{\text{UU}} = \mathbb{E}[|\mathbf{u}_{f,\tau}|^2]$ and $\psi_{f,\tau}^{\text{ZZ}} = \mathbb{E}[|z_{f,\tau}|^2]$, respectively, to the optimum step-size

$$\mu_{l,f,\tau} \leftarrow g^{\text{MB}}(\psi_{f,\tau}^{\text{UU}}, \psi_{f,\tau}^{\text{ZZ}}, \dots) \quad (9)$$

with $g^{\text{MB}}(\cdot)$ denoting a deterministic function. Among the most widely used traditional step-size selection strategies are

- a) the stall-or-adapt NLMS step-size, e.g., [8], [9],

$$\mu_{l,f,\tau} \leftarrow \frac{m_{\tau}^{\text{DT}}}{\psi_{f,\tau}^{\text{UU}}} \quad \forall l \in \{0, \dots, L-1\} \quad (10)$$

with the binary parameter m_{τ}^{DT} being controlled by a double-talk detector,

- b) the error power-aware (EA) NLMS step-size [36], [37]

$$\mu_{l,f,\tau} \leftarrow \frac{m^{\text{EA-NLMS}}}{\psi_{f,\tau}^{\text{UU}} + \psi_{f,\tau}^{\text{EE}}} \quad \forall l \in \{0, \dots, L-1\} \quad (11)$$

²Note that the independent minimization of the frequency band-wise subband error powers requires sufficient suppression of cross-band aliasing to approximate the minimization of the time-domain error power.

with the static hyperparameter $m^{\text{EA-NLMS}} > 0$,

- c) the minimum system-distance NLMS step-size [7]

$$\mu_{l,f,\tau} \leftarrow \frac{\mathbb{E} \left[\left| \left(\mathbf{h}_{f,\tau} - \mathbf{h}_{f,\tau}^{\text{MMSE}} \right)^{\text{T}} \mathbf{u}_{f,\tau} \right|^2 \right]}{\mathbb{E} \left[\left| \left(\mathbf{h}_{f,\tau} - \mathbf{h}_{f,\tau}^{\text{MMSE}} \right)^{\text{T}} \mathbf{u}_{f,\tau} \right|^2 \right] + \psi_{f,\tau}^{\text{ZZ}}} \frac{1}{\psi_{f,\tau}^{\text{UU}}}, \quad (12)$$

for all $l \in \{0, \dots, L-1\}$ with the Minimum Mean Square Error (MMSE) filter estimate $\mathbf{h}_{f,\tau}^{\text{MMSE}}$, and

- d) the Kalman filter step-size [11], [12], [38]

$$\mu_{l,f,\tau} \leftarrow \frac{\Psi_{l,f,\tau}^{\text{HH}}}{\sum_{l=0}^{L-1} \Psi_{l,f,\tau}^{\text{HH}} |u_{f,\tau-l}|^2 + \psi_{f,\tau}^{\text{ZZ}}} \quad (13)$$

with the filter estimation variances $\Psi_{0,f,\tau}^{\text{HH}}, \dots, \Psi_{L-1,f,\tau}^{\text{HH}}$. Note that except for the Kalman update (13), all considered adaptation control methods assume equal step-sizes for updating the filter coefficients within a time-frequency bin. Furthermore, while (10) represents a binary broadband stall-or-adapt step-size, (12) and (13) yield continuous-valued frequency-selective step-sizes. All approaches have in common that they rely on a precise estimation of typically unknown expectations which often depend on non-observable signals, e.g., the interference power $\psi_{f,\tau}^{\text{ZZ}}$ or the MMSE filter estimate $\mathbf{h}_{f,\tau}^{\text{MMSE}}$. Furthermore, the claimed optimality of the respective step-sizes holds only under strong model assumptions, e.g., a linear Gaussian model for the Kalman filter update (13), whose validity is often questionable in practice. To remedy these limitations, we resort now to the concept of deep learning-based step-size estimation.

B. Deep Learning-based Adaptation Control

The general idea of deep learning-based step-size estimation is to replace the mapping $g^{\text{MB}}(\cdot)$ in (9) by a DNN [23]–[25]

$$\boldsymbol{\mu}_{\tau} = (\mu_{1,\tau} \quad \dots \quad \mu_{F,\tau})^{\text{T}} \leftarrow g^{\text{BB-DNN}}(\boldsymbol{\chi}_{\tau}, \boldsymbol{\zeta}_{\tau}; \boldsymbol{\theta}^{\text{BB}}) \quad (14)$$

with parameter vector $\boldsymbol{\theta}^{\text{BB}}$ which infers the frame-dependent broadband step-size vector $\boldsymbol{\mu}_{\tau}$ from an observable feature vector $\boldsymbol{\chi}_{\tau}$ and internal DNN state vector $\boldsymbol{\zeta}_{\tau}$. Note that we assume in Eq. (14) equal step-sizes within a time-frequency bin, i.e., $\forall l \in \{0, \dots, L-1\} : \mu_{f,\tau} = \mu_{f,l,\tau}$, which is common to many adaptation control approaches (cf. Eqs. (10) - (12)).

We now describe three different generic adaptation control strategies which differ in the structure of the DNN-based mapping $g^{\text{BB-DNN}}(\cdot)$. For this we first introduce a decomposition of the broadband feature vector $\boldsymbol{\chi}_{\tau}$ into F narrowband feature vectors $\boldsymbol{\chi}_{f,\tau}$ with $f = 1, \dots, F$, which contain only information about the respective frequency bands as follows:

$$\boldsymbol{\chi}_{\tau} = (\boldsymbol{\chi}_{1,\tau}^{\text{T}} \quad \dots \quad \boldsymbol{\chi}_{F,\tau}^{\text{T}})^{\text{T}}. \quad (15)$$

This forms the input to the following three DNN-based step-size inference approaches:

- a) *Broadband DNN*. The first and simplest method is to jointly infer all F narrowband step-sizes $\mu_{1,\tau}, \dots, \mu_{F,\tau}$, contained in the broadband vector $\boldsymbol{\mu}_{\tau}$, by a single DNN which exploits features from the entire frequency spectrum. This approach is straightforwardly related to the mapping (14) and visualized in Fig. 2a.

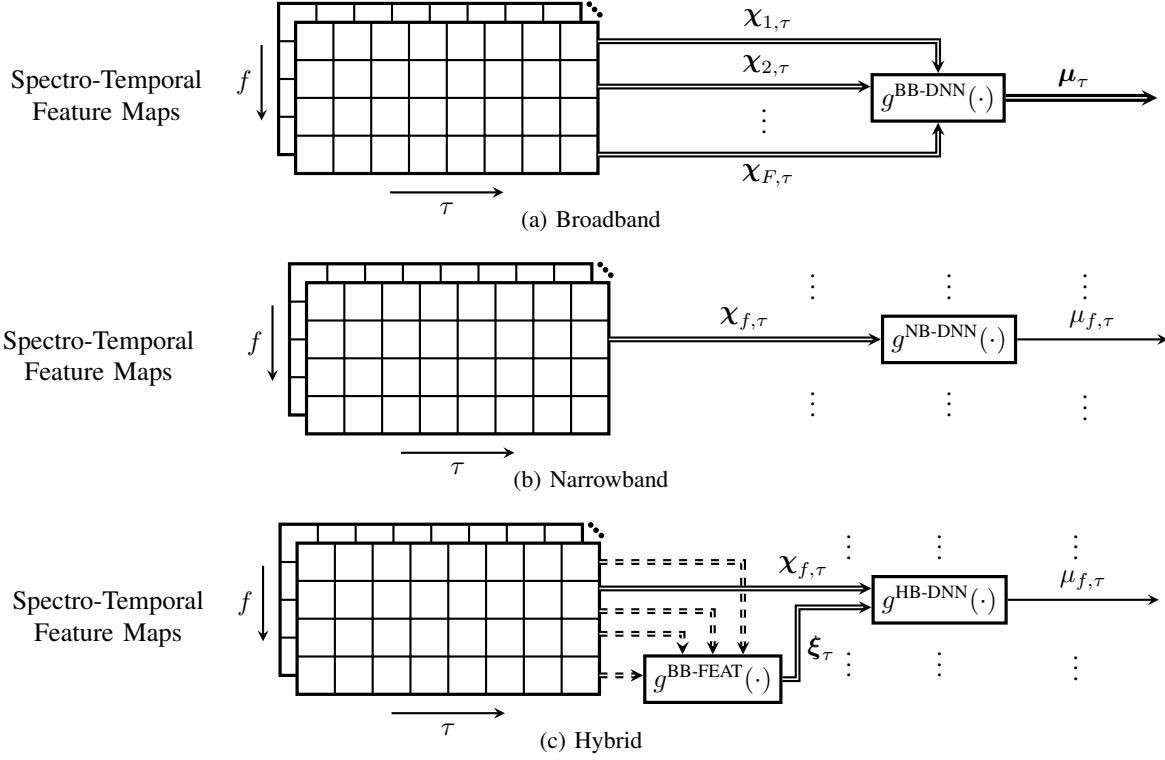


Fig. 2: Narrowband, broadband and hybrid DNN-based adaptation control. While in broadband control a single DNN is used to simultaneously infer a frequency-selective broadband step-size vector μ_τ , narrowband and hybrid approaches use independent DNNs to estimate scalar step-sizes $\mu_{f,\tau}$ per frequency band. While narrowband approaches exploit only information from the respective frequency band, hybrid methods use an additional low-dimensional feature vector ξ_τ which is representative of the entire spectrum. The dashed arrows represent the dependency of the vector ξ_τ on the observations of all frequency bands.

b) *Narrowband DNN*. In many traditional approaches (cf. Sec. III-A) the narrowband step-size $\mu_{f,\tau}$ is computed only from statistics of the respective frequency band, i.e., without exploiting any inter-frequency dependencies. This motivates a decomposition of the general mapping $g^{\text{BB-DNN}}(\cdot)$ in (14) into F narrowband mappings [26], [28], [29]

$$\mu_{f,\tau} \leftarrow g^{\text{NB-DNN}}(\chi_{f,\tau}, \zeta_{f,\tau}; \theta^{\text{NB}}) \quad (16)$$

as shown in Fig. 2b. Eq. (16) suggests an inference of the narrowband step-size $\mu_{f,\tau}$ from a narrowband feature vector $\chi_{f,\tau}$ with $\zeta_{f,\tau}$ and θ^{NB} denoting the internal state and parameter vectors of the DNN, respectively. Note that we assume the DNN parameter vector θ^{NB} to be shared among different frequency bands which significantly reduces the number of trainable DNN parameters. It furthermore offers the possibility to use a single trained DNN for applications with different frequency resolutions which increases the flexibility.

c) *Hybrid DNN*. A possible disadvantage of the narrowband relative to the broadband method is that it cannot exploit statistical inter-frequency dependencies for adaptation control. To remedy this limitation, while still benefiting from the low DNN parameter count of narrowband approaches, we introduce a hybrid of both methods which is shown in Fig. 2c. The key idea is to employ an individual mapping per frequency band, as suggested in the narrowband approach, yet, extend the narrowband feature vector $\chi_{f,\tau}$ by a small number of additional hybrid features which are representative for the

entire frequency spectrum. The respective hybrid step-size mapping is given by

$$\mu_{f,\tau} \leftarrow g^{\text{HB-DNN}}\left(\left(\chi_{f,\tau}^T \quad \xi_\tau^T\right)^T, \zeta_{f,\tau}; \theta^{\text{HB}}\right) \quad (17)$$

with the narrowband feature vector $\chi_{f,\tau}$, the hybrid feature vector ξ_τ , the internal DNN state vector $\zeta_{f,\tau}$ and the parameter vector θ^{HB} . In Fig. 2c the computation of the hybrid feature vector ξ_τ is indicated by the function $g^{\text{BB-FEAT}}(\cdot)$ which does not exhibit any trainable parameters. The benefit of the additional features critically depends on their design which is discussed in Sec. III-C.

Finally, we observe that all three approaches suggest a frequency-selective adaptation control scheme. An alternative is to enforce equivalent step-sizes for all frequency bands which is common to many time-domain LMS-based filter updates. This approach can be directly incorporated into the broadband method (14) by assuming

$$\mu_\tau \leftarrow \mu_\tau \mathbf{1}_F \quad (18)$$

with the scalar step-size μ_τ being provided by the DNN.

C. Feature Vectors

We will now discuss various choices for the narrowband and hybrid feature vectors $\chi_{f,\tau}$ and ξ_τ , respectively, which are used to infer the step-sizes (cf. Eqs. (14) - (17)). The

feature vectors can be computed from any subset of the following observable signals: The loudspeaker signal $u_{f,\tau}$, the microphone signal $y_{f,\tau}$, the error signal $e_{f,\tau}$ and the echo estimate $\hat{d}_{f,\tau}$. As we consider in this paper only real-valued DNNs, each complex-valued signal must be transformed to the field of real numbers. A straightforward mapping is given by stacking the real and imaginary parts of a subset of the complex-valued signals, e.g., the loudspeaker and microphone signals $u_{f,\tau}$ and $y_{f,\tau}$, respectively,

$$\chi_{f,\tau}^T \leftarrow (\mathcal{R}\{u_{f,\tau}\} \ \mathcal{I}\{u_{f,\tau}\} \ \mathcal{R}\{y_{f,\tau}\} \ \mathcal{I}\{y_{f,\tau}\}). \quad (19)$$

Many traditional adaptation control approaches (cf. Sec. III-A) mainly rely on the signal magnitude, i.e., discard the phase information. This motivates a non-linear mapping by the magnitude operator and an additional logarithmic transformation with exemplary narrowband feature vectors being given by

$$\chi_{f,\tau}^T \leftarrow (|u_{f,\tau}| \ |y_{f,\tau}|), \quad (20)$$

$$\chi_{f,\tau}^T \leftarrow (\log_{10}(|u_{f,\tau}| + \delta^{\text{FEAT}}) \ \log_{10}(|y_{f,\tau}| + \delta^{\text{FEAT}})), \quad (21)$$

respectively, with $\delta^{\text{FEAT}} > 0$ being a small constant to avoid numerical instabilities. Note that in principle any combination of signals and transformations can be used to define a narrowband feature vector $\chi_{f,\tau}$. Yet, some combinations might be less promising, considering for example the linear relationship of the microphone, error and echo estimates.

We will now discuss the design of the hybrid feature vector ξ_τ which should be representative for the entire frequency spectrum at time frame τ . Similar to the narrowband feature vector $\chi_{f,\tau}$, it can be computed from a subset of the complex-valued signals $u_{f,\tau}$, $y_{f,\tau}$, $e_{f,\tau}$ and $\hat{d}_{f,\tau}$, yet, now considering all frequency bands. To condense the respective broadband vectors to low-dimensional real-valued scalars, we consider the arithmetic magnitude averages [39]

$$\bar{y}_\tau = \frac{1}{F} \sum_{f=1}^F |y_{f,\tau}| \quad (22)$$

with \bar{e}_τ and \bar{d}_τ being defined accordingly. By stacking a subset of the magnitude averages \bar{y}_τ , \bar{e}_τ and \bar{d}_τ into a vector, we obtain an exemplary hybrid feature vector ξ_τ . As the feature (22) is independent of the frequency resolution, the hybrid method keeps the flexibility benefit, i.e., application to different frequency resolutions, of the narrowband approach. Finally, we note that all feature vectors are normalized to zero mean and unit variance with the respective statistics being estimated during training.

D. Output Layer Design of the DNNs

In Sec. III-B, we discussed the key idea of estimating the step-size $\mu_{f,\tau}$, which controls the CTF filter adaptation (cf. Eq. (7)), by a DNN. Yet, due to the non-whiteness and non-stationarity that many acoustic signals exhibit [40], a direct estimation of the LMS step-size $\mu_{f,\tau}$ requires the DNN to cover a large numerical range in its last layer. To remedy this limitation we enforce a specific structure in the output layer of the DNN. To motivate this structure we first consider the

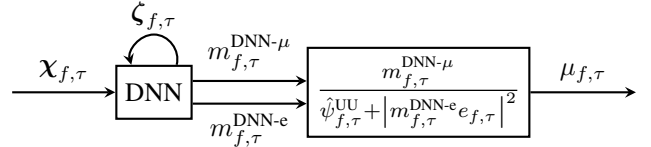


Fig. 3: Block diagram of the proposed DNN-controlled narrowband step-size estimation approach with the DNN-provided masks $m_{f,\tau}^{\text{DNN-}\mu}$ and $m_{f,\tau}^{\text{DNN-e}}$, the feature vector $\chi_{f,\tau}$ and the internal DNN state vector $\zeta_{f,\tau}$.

optimum NLMS step-size (12). We observe that the second part of the product, i.e., the loudspeaker power normalization, is easily estimated by recursive averaging

$$\hat{\psi}_{f,\tau}^{\text{UU}} = \lambda_U \hat{\psi}_{f,\tau-1}^{\text{UU}} + (1 - \lambda_U) \|u_{f,\tau}\|^2 \quad (23)$$

whereas the first part is difficult to estimate, yet, limited to the range $[0, 1]$. Thus, to address the numerical range difficulty, a straightforward idea is to use a sigmoid activation in the output layer of the DNN and subsequently normalize the outcome by the loudspeaker power estimate (23) [23], [24]. Yet, as the basic NLMS update is not interference-robust, the DNN training might be complicated as no guidance is available. In contrast, the traditional step-size estimators (11) - (13) have already been derived with the goal of interference-robustness. To exploit this additional domain knowledge, and therefore potentially simplifying the DNN training, we enforce the following output layer, and thus step-size, structure [23]

$$\mu_{f,\tau} \leftarrow \frac{m_{f,\tau}^{\text{DNN-}\mu}}{\hat{\psi}_{f,\tau}^{\text{UU}} + |m_{f,\tau}^{\text{DNN-e}} e_{f,\tau}|^2 + \delta^{\text{VSS}}} \quad (24)$$

with the DNN-provided masks $m_{f,\tau}^{\text{DNN-}\mu}$ and $m_{f,\tau}^{\text{DNN-e}}$ being limited to the range from 0 to 1 and the small regularization constant $\delta^{\text{VSS}} > 0$. Note that the output layer structure (24) is closely related to the error power-aware NLMS step-size (11) with the DNN providing a frequency- and frame-selective hyperparameter $m^{\text{EA-NLMS}}$ and controlling the error power normalization by $m_{f,\tau}^{\text{DNN-e}}$. By choosing $m_{f,\tau}^{\text{DNN-e}} = 0$ we obtain a DNN-controlled NLMS update similar to [24]. The overall approach, including a narrowband DNN, is shown in Fig. 3.

E. Loss Functions

We now discuss different loss functions for optimizing the broadband, narrowband and hybrid DNN parameter vectors θ^{BB} , θ^{NB} , and θ^{HB} , respectively. Note that we use θ as representative for all three parameter vectors in this section. The relation of the DNN parameter vector θ to the CTF filter estimates $h_{f,\tau}$, STFT-domain echo estimates $\hat{d}_{f,\tau}$ and time-domain echo estimates \hat{d}_κ with the frequency index $f \in \{1, \dots, F\}$, the frame index $\tau \in \{1, \dots, T\}$ and the time-domain sample index $\kappa \in \{1, \dots, K\}$, respectively, is shown in Fig. 4. In general, there are two types of loss functions which differ in their optimization targets: 1) Approximation of oracle target step-sizes, 2) Approximation of the desired echo signal. Possible choices for the desired target step-sizes could be the minimum system distance NLMS or Kalman step-sizes

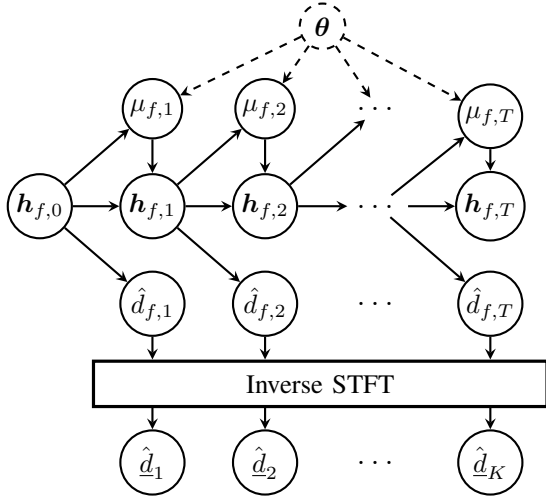


Fig. 4: Relation of the DNN parameter vector θ to the CTF filter estimates $h_{f,\tau}$, STFT-domain echo estimates $\hat{d}_{f,\tau}$ and time-domain echo estimates \hat{d}_κ .

given in Eqs. (12) and (13). Yet, this approach is challenged by the difficulty to design a proper distance measure as the effect of estimation errors on the echo cancellation performance is complicated. Furthermore, as optimum model-based step-sizes are typically derived by certain signal assumptions, e.g., a linear Gaussian observation model within the Kalman filter framework, their *optimality* cannot be guaranteed for realistic data. Therefore, we resort in this paper to the second approach which represents an end-to-end optimization strategy [23]–[29] as it directly quantifies the effect of the step-size estimate on the echo cancellation performance. Considering the different signal domains, i.e., time or frequency domain, we always investigate pairs of loss functions in the following. A first naive choice is given by the Mean Square Error (MSE) losses

$$\mathcal{J}^{\text{FD-MSE}}(\theta) = \frac{1}{TF} \sum_{\tau,f=1}^{T,F} |d_{f,\tau} - \hat{d}_{f,\tau}|^2 \quad (25)$$

$$\mathcal{J}^{\text{TD-MSE}}(\theta) = \frac{1}{K} \sum_{\kappa=1}^K |d_\kappa - \hat{d}_\kappa|^2 \quad (26)$$

with d_κ and \hat{d}_κ denoting the time-domain echo and estimated echo signals at sample index κ , respectively, and K, T denoting the number of time-domain samples and frames, respectively. It should be noted that while the frequency-domain loss (25) suggests an independent residual echo power minimization per frequency band, its time-domain counterpart (26) couples the frequency-wise echo estimates by the inverse STFT. In addition, we examine the negated logarithmic Echo Return Loss Enhancement (ERLE)-type losses

$$\mathcal{J}^{\text{FD-ERLE}}(\theta) = -\log_{10} \frac{\delta^{\text{LOSS}} + \frac{1}{TF} \sum_{\tau,f=1}^{T,F} |d_{f,\tau}|^2}{\delta^{\text{LOSS}} + \frac{1}{TF} \sum_{\tau,f=1}^{T,F} |d_{f,\tau} - \hat{d}_{f,\tau}|^2} \quad (27)$$

$$\mathcal{J}^{\text{TD-ERLE}}(\theta) = -\log_{10} \frac{\delta^{\text{LOSS}} + \frac{1}{K} \sum_{\kappa=1}^K |d_\kappa|^2}{\delta^{\text{LOSS}} + \frac{1}{K} \sum_{\kappa=1}^K |d_\kappa - \hat{d}_\kappa|^2} \quad (28)$$

with $\delta^{\text{LOSS}} > 0$ being a regularization factor to avoid numerical instabilities. Note that the echo powers in the numerators of (27) and (28) do not depend on the DNN parameter vector θ and could therefore be discarded. Nevertheless we keep it here for its analogy with the commonly-used ERLE. Note that the respective MSE and ERLE losses essentially differ in the additional transformation by a logarithm.

IV. EXPERIMENTS

We will now compare the various adaptation control approaches (cf. Sec. III-B), signal feature vector choices (cf. Sec. III-C), output layer designs (cf. Sec. III-D) and loss functions (cf. Sec. III-E) w.r.t. each other and relative to various well-known traditional adaptation control algorithms (cf. III-A) for a variety of challenging acoustic scenarios.

A. Experimental Setup

In this section, we describe the experimental setup which was used to train the DNNs and compare the different adaptation control algorithms. As introduced in Sec. II-A, we consider the microphone signal to be composed of a loudspeaker echo, near-end speech and background noise component (cf. Eq. (1)). The near-end speech signals for the training and test sets were sampled randomly from the *real* (12 h) and *blind test* (1.2 h) data sets, respectively, of the *Microsoft AEC Challenges* [3]–[5], which contains recordings from a variety of acoustic environments and devices. The background noise signals were sampled randomly from the training (150 h) and test sets (17 h) of the *DNS* [41] and the *CHiME3* [42] challenges, respectively. The echo signals were computed by a linear convolution of randomly-selected Loudspeaker-Enclosure-Microphone (LEM) Impulse Responses (IRs) with randomly-selected music or speech loudspeaker signals. The LEM IRs for computing the echo signals in the training data were sampled randomly from the *Microsoft AEC Challenges* [3]–[5] and *MIT Survey* [43] data sets and comprised a total of 1134 measured IRs from a variety of acoustic scenes and devices. Note that [3]–[5] provide only sweep measurements and the respective IRs must be computed in a pre-processing step. The LEM IRs for generating the test echo data were taken from a disjoint subset of [3]–[5] and represented in total 300 different acoustic scenes and devices. The loudspeaker speech and music signals for training were taken from the training subsets of [44] (11.5 h and 919 speakers) and [45], [46] (5.5 h from different genres), respectively. The test speech signals were taken from [44], [47] (2.6 h and 209 speakers) and the music test signals were taken from the test subset of [45], [46] (2.4 h). Note that we refrained from directly taking the recorded echo signals from [3]–[5] as only speech far-end signals are available and many recordings contain high-level fan noise which cannot be attenuated by an echo canceler and thus complicate a proper evaluation. The respective fan noise is typically dealt with by a post filter [1] which we do not consider in this paper, yet, could easily be appended to the discussed echo cancelers³. To investigate the tracking

³Note that fan noise is still considered in the background noise signals from [41] and thus its effect on the adaptation control performance can be assessed.

behaviour of the algorithms, which is of particular interest for mobile devices, we also considered time-varying acoustic scenes. For this, we switched the LEM IRs in 90% of the signals after randomly-selected scene durations in the range from 3 s to 6 s. To include both, hard and smooth transitions, a linear fading with a randomly-selected duration between 0 s to 1 s has been considered. Furthermore, two thirds of the loudspeaker and near-end speech signals were pre-processed by a temporal masking with random onsets and offsets to mimic conversations with non- and partially overlapping activity. Finally, the signals were scaled to obtain random *near-end-to-echo* and *near-end-to-echo-and-noise* power ratios in the ranges $[-10, 10]$ dB and $[20, 40]$ dB, respectively, and unit loudspeaker/microphone variances. Note that the respective power estimates were computed only over segments with considerable signal activity to limit the effect of pauses. All signals were sampled at a sampling frequency of 16 kHz and limited to a duration of 8 s. In total, we used 6 h of training data, 1.5 h of validation data and 1 h of testing data. Note that the LEM IRs, speech, music and noise signals of the test data are disjoint from the training/validation data sets.

B. Algorithmic Settings

We now discuss the parameter settings of the various algorithms. The frame shift and DFT length of the STFT were chosen to 128 and 512, respectively, and the Hamming window has been applied prior to transformation⁴. The CTF filter length L was set to 8 which covers approximately 88 ms of the corresponding LEM IRs.

1) *Deep Learning-based Adaptation Control*: The DNN architecture was composed of a fully connected layer with a leaky RELU activation, two stacked Gated Recurrent Unit (GRU) layers and two parallel fully connected layers with sigmoid activations which map from the GRU states to the different adaptation control masks $m_{f,\tau}^{\text{DNN-}\mu}$ and $m_{f,\tau}^{\text{DNN-e}}$, respectively that define the step-size (cf. Eq. (24)). This commonly used architecture was chosen to encode important information about the near-end speech/background noise activity and filter convergence state from the feature sequence within the GRU states. Note that the proposed method is not limited to this architecture and other architectures can straightforwardly be embedded. The recursive loudspeaker power estimation factor and the various regularization constants are chosen to $\lambda_U = 0.9$, $\delta^{\text{FEAT}} = \delta^{\text{LOSS}} = 10^{-12}$ and $\delta^{\text{VSS}} = 10^{-3}$, respectively. The dimension of the GRU states was set to 128 for the broadband step-size estimator (cf. Eq. (14)) and to 64 for the narrowband and hybrid estimators (cf. Eqs. (16) and (17)), respectively. Note that the GRU dimensions have been chosen differently to account for the respective task difficulties, i.e., estimation of a step-size vector μ_τ in comparison to a scalar step-size $\mu_{f,\tau}$. The DNNs were trained for 60 epochs with the ADAM optimizer [48], a step-size of 10^{-3} and an early stopping after 20 epochs with no performance improvement on the validation data. Furthermore, the ADAM step-size was decreased by one-half after five consecutive epochs with no

performance improvement, and Euclidean norm-based gradient clipping with a threshold of 0.5 was applied. The batch size was chosen as 4 and 32 for the narrowband/hybrid and broadband methods, respectively, to account for hardware memory requirements. Finally, the optimum model was selected based on the lowest training loss on the validation data.

2) *Traditional and Oracle Adaptation Control*: To assess the performance of the proposed deep learning-based adaptation control algorithms, we consider various widely-used traditional step-size estimation algorithms. In particular, we consider the error power-aware NLMS algorithm [36], [37], denoted by *EA-NLMS* (cf. Eq. (11)), and the narrowband CTF Kalman filter update [11], [12], [38], denoted by *KF* (cf. Eq. (13)). The interference power $\psi_{f,\tau}^{ZZ}$ and the error power $\psi_{f,\tau}^{EE}$ which are required for the respective updates are both estimated by recursive averaging of the magnitude-squared error $|e_{f,\tau}|^2$ with a smoothing factor of 0.5 [18]. Furthermore, the raw step-size $m^{\text{EA-NLMS}}$ and loudspeaker smoothing parameter λ_U of the *EA-NLMS* algorithm were chosen to 0.2 and 0.9, respectively, and the state transition factor and initial filter estimation variances of the Kalman filter update are chosen to 0.99 and 1, respectively. The filter process noise power for the Kalman filter was chosen proportionally to a temporally-smoothed average of the magnitude-squared filter coefficients as described in [12]. In addition, an additive regularization of 10^{-3} was added to the numerators of the *EA-NLMS* and *KF* updates (cf. Eqs. (11) and (13)) and a minimum filter process noise power of 10^{-3} was chosen for the Kalman filter which drastically improved their robustness. Note that the hyperparameters have been optimized by a grid search on the test data set which favors the baseline results.

Besides the traditional step-size estimators, we consider also two oracle baselines which have knowledge about the individual signal components. On the one hand, we consider an oracle NLMS algorithm, denoted by *Oracle-Grad-NLMS*, which uses the true echo component $d_{f,\tau}$ instead of the microphone signal $y_{f,\tau}$ to compute the CTF filter gradient (cf. Eqs. (2) and (7)). On the other hand, an interference power (IP)-informed Kalman filter approach, denoted by *Oracle-IP-KF*, is investigated which estimates the interference power $\psi_{f,\tau}^{ZZ}$ by a recursive average of the magnitude-squared interfering signal $|z_{f,\tau}|^2 = |s_{f,\tau} + n_{f,\tau}|^2$ with a smoothing parameter of 0.5. It is important to note that while *Oracle-Grad-NLMS* uses the true echo signal for computing the CTF filter update, and therefore adapts continuously, *Oracle-IP-KF* exploits only oracle knowledge about the interference power for computing the step-size, and therefore does not adapt continuously. The step-size of *Oracle-Grad-NLMS* was chosen to 0.2 and the loudspeaker power was estimated by recursive averaging with a smoothing parameter of $\lambda_U = 0.9$. Furthermore, a regularization constant of 10^{-3} was added to the numerator of the update. The state transition factor, initial filter estimation variances, minimum process noise power and additive regularization of *Oracle-IP-KF* were chosen to 0.999, 0.1, 10^{-4} and 1, respectively. Finally, note that the results of both oracle algorithms do not pose an upper performance bound for the linear CTF echo estimation model (3) as the hyperparameters are frequency independent and have been chosen equivalently

⁴Note that a quarter-frameshift is chosen to attain sufficient cross-band attenuation.

for all acoustic scenes of the test data set, based on the best average performance.

C. Performance Measures

We now introduce various measures to compare the performance of the different adaptation control algorithms. One of the most popular measures is given by the ERLE [2]

$$\text{ERLE} = 10 \log_{10} \frac{\sum_{\kappa=1}^K \underline{d}_{\kappa}^2}{\sum_{\kappa=1}^K (\underline{d}_{\kappa} - \hat{\underline{d}}_{\kappa})^2} \quad (29)$$

which is computed by the logarithmic ratio of the time-domain echo power relative to the residual echo power after the echo canceler. It is important to note that the ERLE definition (29) considers the true echo signal \underline{d}_{κ} and not the microphone signal \underline{y}_{κ} and thus can also be used to assess the echo power attenuation during double-talk. Furthermore, it is, apart from regularization constants, equivalent to the negated loss function (28). Due to its simple interpretability, the ERLE is widely used in practice. Yet, it does not consider the characteristics of the possibly distorted desired near-end speech signal. Thus, we additionally introduce the Perceptual Evaluation of Speech Quality (PESQ) [49]

$$\text{PESQ} = f^{\text{PESQ}}(\underline{s}_{\kappa}, \underline{s}_{\kappa} + \underline{d}_{\kappa} - \hat{\underline{d}}_{\kappa}) \quad (30)$$

with the residual echo $\underline{d}_{\kappa} - \hat{\underline{d}}_{\kappa}$ representing an additive distortion. Note that we refrained from considering the background noise component \underline{n}_{κ} in (30) as it cannot be canceled by the echo canceler and thus only dilutes the comparability.

D. Evaluation

In the following, the different adaptation control algorithms are compared w.r.t. their performance on the 450 acoustic scenes of the test data set (cf. Sec. IV-A). We always provide mean and standard deviation in the format *mean/std* with the best measure of each algorithmic class being typeset in bold font. For ease of readability, we abbreviate the DNN-based adaptation control algorithms in the results tables by Broadband (BB), Narrowband (NB) and Hybrid (HB), respectively.

1) *Number of DNN Parameters and Runtime*: We start by comparing the algorithms in terms of DNN parameter count, runtime t_{proc} to process a single STFT block of length 32 ms and Real Time Factor (RTF). Tab. I shows the respective measures for the considered traditional and deep learning-based adaptation control algorithms. The block processing runtime t_{proc} and RTF have been measured on an *Intel Xeon W-1390@2.80GHz* CPU. Note that all presented values depend on the specific algorithmic configuration, i.e., dimensions of

TABLE I: Approximate number of DNN parameters, block processing runtime t_{proc} and RTF for a typical configuration of the different adaptation control approaches.

	EA-NLMS	KF	BB-DNN	NB-DNN	HB-DNN
#Parameters	—	—	$330 \cdot 10^3$	$50 \cdot 10^3$	$50 \cdot 10^3$
t_{proc} in ms	0.11	0.15	0.59	0.79	0.83
RTF	0.014	0.018	0.074	0.098	0.10

the signal feature vectors and GRU states. Thus, the values can only be considered as typical representatives of the respective algorithmic class. Obviously the broadband deep learning-based adaptation control (BB-DNN) exhibits significantly more parameters than the narrowband (NB-DNN) and hybrid (HB-DNN) versions which is straightforwardly explained by the larger feature, masking and GRU dimensions. Furthermore, the narrowband and hybrid DNNs exhibit a similar number of DNN parameters as they differ only by an additional fully connected layer, with at most 192 parameters, which maps from the hybrid feature vector $\underline{\xi}_{\tau}$ to the GRU states (cf. Fig. 2). Considering the runtime, the DNN-based algorithms are approximately four to seven times slower than their traditional counterparts with the hybrid method exhibiting the highest runtime. Yet, it should be noted that the runtime of all algorithms could easily be reduced by subsampling the step-size inference, i.e., keeping it constant for several successive frames. This is in particular attractive for an STFT with a quarter-frameshift as considered in this paper. Finally, it might seem counterintuitive that the broadband method has a lower processing runtime than the narrowband/hybrid methods, despite exhibiting more parameters. Yet, this is straightforwardly explained by considering that the broadband approach requires only a single DNN inference to jointly estimate the step-sizes for all frequency bands while the narrowband and hybrid methods execute individual DNN inferences per frequency band.

2) *Loss Functions*: We now investigate the different loss functions for DNN training that have been introduced in Sec. III-E. Tab. II shows the performance evaluation for the broadband, narrowband and hybrid DNN-based adaptation control algorithms after being trained with the different loss functions (25) - (28). As feature vectors we considered the absolute STFT-domain loudspeaker and microphone signals and the DNN output layer was chosen according to (24). We

TABLE II: Loss function comparison for broadband (BB), narrowband (NB) and hybrid (HB) DNN-based adaptation control algorithms with the absolute STFT-domain loudspeaker and microphone signals as feature vectors.

Loss (Eq.)	Structure	ERLE	PESQ
FD-MSE (25)	BB-DNN	12.79/3.1	1.93/0.8
	NB-DNN	14.54/3.3	2.11 /0.8
	HB-DNN	14.66 /3.3	2.11 /0.8
TD-MSE (26)	BB-DNN	12.84/3.2	1.92/0.8
	NB-DNN	14.48/3.3	2.10/0.8
	HB-DNN	14.61 /3.3	2.11 /0.8
FD-ERLE (27)	BB-DNN	12.78/3.5	1.94/0.8
	NB-DNN	14.51/3.4	2.10/0.8
	HB-DNN	14.70 /3.4	2.12 /0.8
TD-ERLE (28)	BB-DNN	12.99/3.3	1.94/0.8
	NB-DNN	14.71/3.4	2.12 /0.8
	HB-DNN	14.85 /3.4	2.12 /0.8
EA-NLMS KF		10.16/3.3	1.81/0.7
		11.99 /3.4	1.96 /0.7
Oracle-IP-KF		14.90/3.6	2.16/0.8
Oracle-Grad-NLMS		15.17 /3.7	2.20 /0.9

TABLE III: Comparison of different feature transformations (cf. Eqs. (19) - (21)) for broadband (BB) and narrowband (NB) deep learning-based adaptation control.

Structure	Feature Mapping	ERLE	PESQ
BB-DNN	$(\mathcal{R}\{\cdot\}, \mathcal{I}\{\cdot\})$	11.59/3.2	1.85/0.7
	$ \cdot $	12.99 /3.3	1.94 /0.8
	$\log_{10}(\cdot + \delta^{\text{FEAT}})$	12.88/3.4	1.94 /0.8
NB-DNN	$(\mathcal{R}\{\cdot\}, \mathcal{I}\{\cdot\})$	14.67/3.4	2.12 /0.8
	$ \cdot $	14.71 /3.4	2.12 /0.8
	$\log_{10}(\cdot + \delta^{\text{FEAT}})$	14.66/3.4	2.12 /0.8

conclude from Tab. II that all deep learning-based step-size estimators (cf. rows 1–4) outperform the traditional error power-aware NLMS and Kalman filter baselines (cf. EA-NLMS and KF) in terms of ERLE. Among the DNN-based step-size estimators, the narrowband and hybrid methods outperform their broadband counterparts by approximately 1.7 dB ERLE and 0.17 PESQ on average. It might seem counterintuitive that the narrowband and hybrid models perform better than the broadband approach despite having much fewer DNN parameters (cf. Tab. I). Yet, it should be noted again that both the narrowband and the hybrid algorithms use individual DNNs, with different internal states, per frequency band. Considering the various loss functions, we observe only minor differences with small benefits for the TD-ERLE cost function (28). Thus, we conclude that the different deep learning-based adaptation control algorithms are highly robust w.r.t. the cost function choice and choose the TD-ERLE cost function (28) for the following experiments.

3) *DNN Feature Vectors*: In this section, the influence of the feature vector choice (cf. Sec. III-C) on the echo cancellation performance is investigated. We first examine the different transformations for mapping from the complex-valued signals to real-valued features. Tab. III shows the average performance measures of the narrowband and broadband DNN-based step-size estimators for the real- and imaginary (cf. Eq. (19)), magnitude (cf. Eq. (20)) and logarithmic magnitude (cf. Eq. (21)) transformations of the complex-valued loudspeaker and microphone signals. We conclude that all feature transformations perform similar for the narrowband method. In contrast, a clear benefit for the magnitude-based features in comparison to the real and imaginary features can be observed for the broadband method. This might be surprising as the latter contain the most information and the magnitude could be computed from the real and imaginary components. Yet, this might require more powerful DNNs architectures. It indicates also that the phase information is less relevant for adaptation control which is also suggested by many traditional step-size estimators (cf. Eqs. (10) - (12)). In addition, it should be considered that the feature dimension of the real and imaginary feature vector is twice the dimension of the magnitude-based feature vectors. As the simple magnitude transformation tends to perform best, it is chosen as basis for the subsequent investigations.

We now examine the effect of different signal choices for computing the magnitude-based features. The average performance measures of the accordingly trained broadband, narrow-

TABLE IV: Comparison of different magnitude-based signal features for broadband (BB), narrowband (NB) and hybrid (HB) DNN-based adaptation control algorithms.

Structure	Features							ERLE	PESQ
	u_f	y_f	e_f	\hat{d}_f	\bar{y}	\bar{e}	\bar{d}		
BB-DNN	✓	✓						12.99/3.3	1.94/0.8
	✓		✓					13.49/3.5	1.99/0.8
		✓	✓	✓				13.35/3.5	1.98/0.8
	✓	✓	✓					13.71/3.5	2.00/0.8
	✓	✓	✓	✓				14.04 /3.4	2.03 /0.8
NB-DNN	✓	✓						14.71/3.4	2.12/0.8
	✓		✓					14.60/3.5	2.13/0.8
		✓	✓	✓				14.71/3.4	2.12/0.8
	✓	✓	✓					15.10/3.5	2.15/0.8
	✓	✓	✓	✓				15.17 /3.5	2.16 /0.8
HB-DNN	✓	✓			✓			14.85/3.4	2.12/0.8
	✓		✓			✓		14.80/3.6	2.13/0.8
		✓	✓		✓	✓		15.35/3.5	2.16/0.8
	✓	✓	✓	✓	✓	✓		15.60 /3.5	2.18 /0.8
	EA-NLMS KF								10.16/3.3
Oracle-IP-KF Oracle-Grad-NLMS								14.90/3.6	2.16/0.8
								15.17 /3.7	2.20 /0.9

band and hybrid DNN-based adaptation control algorithms is shown in Tab. IV. We observe that in general increasing the feature set improves the adaptation control performance. In particular, the joint usage of the microphone and the error signal seems to be beneficial. This might be explained by the importance of the convergence state information of the echo canceler that is difficult to extract from the respective individual signals. We finally observe that the best-performing DNN-based step-size estimator outperforms the oracle NLMS method in terms of ERLE and almost attains its PESQ values. Yet, it should be noted again that both oracle algorithms assume equivalent (frequency independent) hyperparameters for all acoustic scenes of the test data set.

4) *Output Layer Design*: Finally, we investigate different output layer designs of the DNN (Sec. III-D). In particular, we examine the effect of omitting the adaptive error power normalization in Eq. (24) by setting $m_{f,\tau}^{\text{DNN-e}} = 0$ or a non-adaptive selection by setting $m_{f,\tau}^{\text{DNN-e}} = 1$. Furthermore, we evaluate a frequency-independent selection of the step-size masks $m_{f,\tau}^{\text{DNN-}\mu}$ and $m_{f,\tau}^{\text{DNN-e}}$, respectively, for the broadband method, i.e., an identical choice for all frequency bands. As feature vectors we use the magnitude loudspeaker, microphone and error signals which showed good performance according to Tab. IV. The respective ERLE and PESQ results are shown in Tab. V. We conclude that frequency-selective step-size masks significantly outperform a frequency-independent choice (cf. BB-DNN) which can be explained by the non-whiteness which is typical for speech and audio signals, both as desired signals and as interference. Furthermore, a general error power normalization within the output layer of the broadband approach, either controlled by a DNN (cf. $m_{f,\tau}^{\text{DNN-e}}=\text{selective}$) or a static choice (cf. $m_{f,\tau}^{\text{DNN-e}}=1$), is beneficial in comparison to a simple DNN-controlled NLMS (cf. $m_{f,\tau}^{\text{DNN-e}}=0$). Yet, the DNN seems to infer values close to one as $m_{f,\tau}^{\text{DNN-e}}=\text{selective}$

TABLE V: Comparison of different output layer designs (cf. Eq. (24)) for DNN-based step-size estimation. While *selective* approaches estimate a different mask for each frequency band, *non-selective* methods estimate a frequency-independent mask which is equivalently applied to all frequency bands.

Structure	Output layer		ERLE	PESQ
	$m_{f,\tau}^{\text{DNN-}\mu}$	$m_{f,\tau}^{\text{DNN-e}}$		
BB-DNN	Selective	Selective	13.71 /3.5	2.00/0.8
	Selective	0	13.03/3.5	1.95/0.8
	Selective	1	13.70/3.4	2.01 /0.8
	Non-Selective	Non-Selective	12.97/3.4	1.90/0.7
	Non-Selective	0	11.45/3.8	1.76/0.7
	Non-Selective	1	12.87/3.3	1.89/0.7
NB-DNN	Selective	Selective	15.10 /3.5	2.15 /0.8
	Selective	0	15.07/3.5	2.15 /0.8
	Selective	1	14.92/3.4	2.14/0.8
HB-DNN	Selective	Selective	15.35 /3.5	2.16 /0.8
	Selective	0	15.30/3.5	2.16 /0.8
	Selective	1	15.13/3.5	2.16 /0.8

and $m_{f,\tau}^{\text{DNN-e}}=1$ show a similar performance. In contrast, no clear benefit of the adaptive error-power normalization within the narrowband and hybrid approaches can be observed. This might be a result of the step-size inference by individual DNNs per frequency band which can handle for the considered architectures more challenging situations in comparison to the broadband approach. Thus, a more conservative, i.e., smaller, step-size choice by error power normalization is not required.

E. Visual Interpretation

After comparing the various approaches numerically, we will now visually interpret the DNN-based step-size estimates. For this we show in Fig. 5 the logarithmic interference, i.e., summed near-end speech and background noise, echo and residual echo signal power spectrograms relative to the DNN-provided step-size mask $m_{f,\tau}^{\text{DNN-}\mu}$ for a specific sequence. Note that around 3.1 s an echo path change occurs which is indicated by the vertical red lines. A broadband approach without any error-power normalization, i.e., $m_{f,\tau}^{\text{DNN-e}} = 0$, and only a single GRU layer with 128 internal states was used to create the results. The stacked magnitude loudspeaker, microphone and error signals were used as feature vectors. To gain more insights into what the DNN actually learns, we additionally try to find similar GRU state vectors across temporally different frames [50]. For this we cluster the respective GRU state vectors of the sequence by agglomerative clustering with the city block metric into two different clusters [51]. Subfig. 5e shows the frame-based assignment of the internal GRU state vectors to the two different classes. We observe from the cluster assignment results in Subfig. 5e that the first class indicates error signal frames which are dominated by interference, i.e., near-end speech or background noise (or no echo activity), whereas the second cluster indicates error signal frames which are dominated by residual echo. Thus, we conclude that the GRU states encode important information about the interference activity which points to the interpretation that the DNN includes a refined double-talk detector. The step-size vectors (columns in Subfig. 5d)

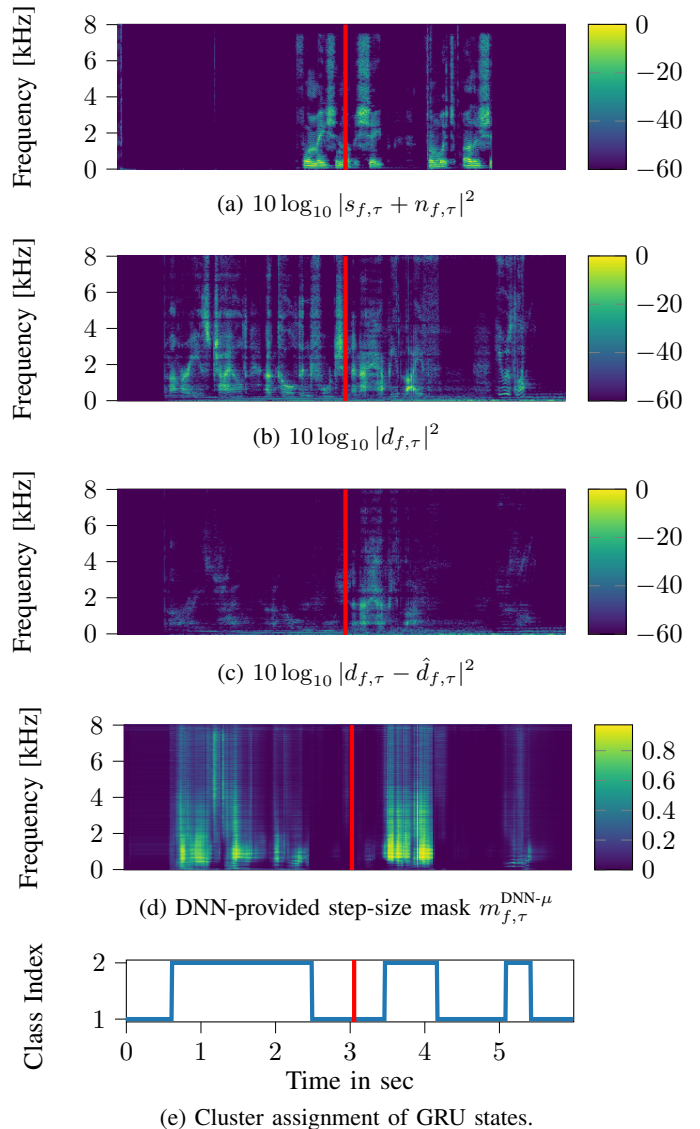


Fig. 5: Logarithmic interference, echo and residual echo power spectrograms in comparison to the DNN-provided step-size mask $m_{f,\tau}^{\text{DNN-}\mu}$ with the red line indicating an echo path change. In Subfig. 5e, the frame-based assignment of the internal GRU states of the DNN to two different classes/clusters is shown.

which are computed from the GRU states of the second cluster exhibit a clear *low-pass* structure, i.e., high-values in the low frequency range, which is reasonable considering the speech loudspeaker signal. Of particular interest is the step-size selection after the echo path change: While there is no adaptation during the initial double-talk period from 3.1 s – 3.5 s, the subsequent decreasing interference power results in high step-sizes and thus rapid filter updates.

V. CONCLUSION

In this paper, we investigated various DNN-based adaptation control methods for frequency domain acoustic echo cancellation. In particular, we compared broadband and narrowband step-size inference approaches and proposed a hybrid method which combines the best out of both worlds. Our results

show significant performance improvements of deep learning-based step-size estimation relative to traditional approaches, in particular for dynamic acoustic scenes. Furthermore, we provide a general view on different signal feature vectors, cost functions and DNN output layers which yields novel insights and guidelines for the design of other deep learning-based adaptation control algorithms. As future work, our generic step-size adaptation approach can be applied to unsupervised system identification applications, e.g., relative transfer function estimation, and to the joint control of various algorithmic components of a multichannel hands-free speech interface, e.g., echo canceler, beamformer and spectral postfilter, by a single DNN as outlined in [25].

REFERENCES

- [1] E. Hänsler and G. Schmidt, *Acoustic Echo and Noise Control: A practical Approach*. NJ, USA: Wiley-Interscience, 2004.
- [2] G. Enzner, H. Buchner, A. Favrot, and F. Kuech, "Acoustic Echo Control," in *Academic Press Library in Signal Processing*. Florida, USA: Elsevier, 2014, vol. 4, pp. 807–877.
- [3] K. Sridhar, R. Cutler, A. Saabas, T. Parnamaa, M. Loide, H. Gamper, S. Braun, R. Aichner, and S. Srinivasan, "ICASSP 2021 Acoustic Echo Cancellation Challenge: Datasets, testing framework, and results," in *IEEE International Conference on Acoustics, Speech and Signal Processing (ICASSP)*, Toronto, Canada, Jun. 2021, pp. 151–155.
- [4] R. Cutler, A. Saabas, T. Parnamaa, M. Loide, S. Sootla, M. Purin, H. Gamper, S. Braun, K. Sorensen, R. Aichner, and S. Srinivasan, "Interspeech 2021 Acoustic Echo Cancellation Challenge," in *Interspeech*, Brno, Czech Republic, Aug. 2021.
- [5] R. Cutler, A. Saabas, T. Parnamaa, M. Purin, H. Gamper, S. Braun, K. Sorensen, and R. Aichner, "ICASSP 2022 Acoustic Echo Cancellation Challenge," in *IEEE International Conference on Acoustics, Speech and Signal Processing (ICASSP)*, Singapore, Singapore, May 2022, pp. 9107–9111.
- [6] S. Haykin, *Adaptive filter theory*, 4th ed. Upper Saddle River, New Jersey: Prentice Hall, 2002.
- [7] A. Mader, H. Puder, and G. U. Schmidt, "Step-size control for acoustic echo cancellation filters – An overview," *Signal Processing*, vol. 80, no. 9, pp. 1697–1719, 2000.
- [8] T. Gansler, M. Hansson, C.-J. Ivarsson, and G. Salomonsson, "A double-talk detector based on coherence," *IEEE Transactions on Communications*, vol. 44, no. 11, pp. 1421–1427, 1996.
- [9] J. Benesty, D. Morgan, and J. Cho, "A new class of doubletalk detectors based on cross-correlation," *IEEE Transactions on Speech and Audio Processing*, vol. 8, no. 2, pp. 168–172, 2000.
- [10] B. H. Nitsch, "A frequency-selective stepfactor control for an adaptive filter algorithm working in the frequency domain," *Signal Processing*, vol. 80, no. 9, pp. 1733–1745, Sep. 2000.
- [11] G. Enzner and P. Vary, "Frequency-domain adaptive Kalman filter for acoustic echo control in hands-free telephones," *Signal Processing*, vol. 86, no. 6, pp. 1140–1156, 2006.
- [12] F. Kuech, E. Mabande, and G. Enzner, "State-space architecture of the partitioned-block-based acoustic echo controller," in *IEEE International Conference on Acoustics, Speech and Signal Processing (ICASSP)*, Florence, Italy, May 2014, pp. 1295–1299.
- [13] J. Benesty, H. Rey, L. Vega, and S. Tressens, "A Nonparametric VSS NLMS Algorithm," *IEEE Signal Processing Letters*, vol. 13, no. 10, pp. 581–584, Oct. 2006.
- [14] J.-M. Valin, "On Adjusting the Learning Rate in Frequency Domain Echo Cancellation With Double-Talk," *IEEE Transactions on Audio, Speech and Language Processing*, vol. 15, no. 3, pp. 1030–1034, Mar. 2007.
- [15] F. Nesta, T. S. Wada, and B. Juang, "Batch-online semi-blind source separation applied to multi-channel acoustic echo cancellation," *IEEE/ACM Transactions on Audio, Speech, and Language Processing*, vol. 19, no. 3, pp. 583–599, 2011.
- [16] J. Gunther, "Learning Echo Paths During Continuous Double-Talk Using Semi-Blind Source Separation," *IEEE/ACM Transactions on Audio, Speech, and Language Processing*, vol. 20, no. 2, pp. 646–660, 2012.
- [17] G. Cheng, L. Liao, H. Chen, and J. Lu, "Semi-Blind Source Separation for Nonlinear Acoustic Echo Cancellation," *IEEE Signal Processing Letters*, vol. 28, pp. 474–478, 2021.
- [18] F. Yang, G. Enzner, and J. Yang, "Frequency-Domain Adaptive Kalman Filter With Fast Recovery of Abrupt Echo-Path Changes," *IEEE Signal Processing Letters*, vol. 24, no. 12, pp. 1778–1782, Dec. 2017.
- [19] T. Haubner, A. Brendel, M. Elminshawi, and W. Kellermann, "Noise-robust adaptation control for supervised acoustic system identification exploiting a noise dictionary," in *IEEE International Conference on Acoustics, Speech and Signal Processing (ICASSP)*, Toronto, Canada, June 2021, pp. 945–949.
- [20] T. Haubner, M. M. Halimeh, A. Brendel, and W. Kellermann, "A synergistic kalman- and deep postfiltering approach to acoustic echo cancellation," in *European Signal Processing Conference (EUSIPCO)*, Dublin, Ireland, August 2021, pp. 990–994.
- [21] A. Ivry, I. Cohen, and B. Berdugo, "Deep adaptation control for acoustic echo cancellation," in *IEEE International Conference on Acoustics, Speech and Signal Processing (ICASSP)*, Singapore, Singapore, May 2022.
- [22] O. Schwartz and A. Schwartz, "RNN-based step-size estimation for the RLS algorithm with application to acoustic echo cancellation," in *IEEE International Conference on Acoustics, Speech and Signal Processing (ICASSP)*, Rhodes Island, Greece, June 2023.
- [23] T. Haubner, A. Brendel, and W. Kellerman, "End-To-End Deep Learning-Based Adaptation Control for Frequency-Domain Adaptive System Identification," in *IEEE International Conference on Acoustics, Speech and Signal Processing (ICASSP)*, Singapore, Singapore, May 2022, pp. 766–770.
- [24] H. Zhang, S. Kandadai, H. Rao, M. Kim, T. Pruthi, and T. Kristjansson, "Deep Adaptive AEC: Hybrid of Deep Learning and Adaptive Acoustic Echo Cancellation," in *IEEE International Conference on Acoustics, Speech and Signal Processing (ICASSP)*, Singapore, Singapore, May 2022, pp. 756–760.
- [25] T. Haubner and W. Kellermann, "Deep Learning-Based Joint Control of Acoustic Echo Cancellation, Beamforming and Postfiltering," in *European Signal Processing Conference (EUSIPCO)*, Belgrade, Serbia, August 2022.
- [26] J. Casebeer, N. J. Bryan, and P. Smaragdus, "Meta-AF: Meta-Learning for Adaptive Filters," *IEEE/ACM Transactions on Audio, Speech, and Language Processing*, vol. 31, pp. 355–370, February 2023.
- [27] J. Wu, J. Casebeer, N. J. Bryan, and P. Smaragdus, "Meta-Learning for Adaptive Filters with higher-order Frequency Dependencies," in *International Workshop on Acoustic Signal Enhancement (IWAENC)*, Bamberg, Germany, September 2022.
- [28] D. Yang, F. Jiang, W. Wu, X. Fang, and M. Cao, "Low-complexity acoustic echo cancellation with neural kalman filtering," in *IEEE International Conference on Acoustics, Speech and Signal Processing (ICASSP)*, Rhodes Island, Greece, June 2023.
- [29] Y. Zhang, M. Yu, H. Zhang, D. Yu, and D. Wang, "NeuralKalman: A Learnable Kalman Filter for Acoustic Echo Cancellation," Feb. 2023, arXiv:2301.12363.
- [30] W. Kellermann, "Analysis and design of multirate systems for cancellation of acoustical echoes," in *IEEE International Conference on Acoustics, Speech and Signal Processing (ICASSP)*, New York, USA, Apr. 1988, pp. 2570–2573.
- [31] P. S. Diniz, *Adaptive Filtering: Algorithms and Practical Implementation*, 4th ed. Springer US, 2012.
- [32] Y. Avargel and I. Cohen, "System Identification in the Short-Time Fourier Transform Domain With Crossband Filtering," *IEEE Transactions on Audio, Speech and Language Processing*, vol. 15, no. 4, pp. 1305–1319, May 2007.
- [33] J. Franzen, E. Seidel, and T. Fingscheidt, "AEC in a nutshell: On target and topology choices for FCRN acoustic echo cancellation," in *IEEE International Conference on Acoustics, Speech and Signal Processing (ICASSP)*, Toronto, Canada, June 2021, pp. 156–160.
- [34] E. Seidel, J. Franzen, M. Strake, and T. Fingscheidt, "Y2-net FCRN for acoustic echo and noise suppressio," in *Interspeech*, Brno, Czechia, August 2021.
- [35] S. Braun and M. L. Valero, "Task splitting for dnn-based acoustic echo and noise removal," in *2022 International Workshop on Acoustic Signal Enhancement (IWAENC)*, Bamberg, Germany, Sep. 2022.
- [36] J. E. Greenberg, P. M. Zurek, and M. Brantley, "Evaluation of feedback-reduction algorithms for hearing aids," *The Journal of the Acoustical Society of America*, vol. 108, no. 5, pp. 2366–2376, Nov. 2000.
- [37] A. Spriet, S. Doclo, M. Moonen, and J. Wouters, "Feedback control in hearing aids," *Springer Handbook of Speech Processing*, pp. 979–1000, 2008.
- [38] M. L. Valero, "Acoustic echo reduction for multiple loudspeakers and microphones: Complexity reduction and convergence en-

- hancement,” doctoral thesis, Friedrich-Alexander-Universität Erlangen-Nürnberg (FAU), 2019.
- [39] A. Schwarz, C. Hofmann, and W. Kellermann, “Spectral feature-based nonlinear residual echo suppression,” in *IEEE Workshop on Applications of Signal Processing to Audio and Acoustics*, New Paltz, NY, USA, Oct. 2013.
- [40] P. Vary and R. Martin, *Digital Speech Transmission*. John Wiley & Sons, 2006.
- [41] H. Dubey, A. Aazami, V. Gopal, B. Naderi, S. Braun, R. Cutler, H. Gamper, M. Golestaneh, and R. Aichner, “Deep speech enhancement challenge at ICASSP 2023,” in *IEEE International Conference on Acoustics, Speech and Signal Processing (ICASSP)*, Rhodes Island, Greece, June 2023.
- [42] J. Barker, R. Marxer, E. Vincent, and S. Watanabe, “The third ‘chime’ speech separation and recognition challenge: Dataset, task and baselines,” in *IEEE Workshop on Automatic Speech Recognition and Understanding (ASRU)*, Scottsdale, Arizona, USA, Dec. 2015, pp. 504–511.
- [43] J. Traer and J. H. McDermott, “Statistics of natural reverberation enable perceptual separation of sound and space,” *Proceedings of the National Academy of Sciences*, vol. 113, no. 48, 2016.
- [44] V. Panayotov, G. Chen, D. Povey, and S. Khudanpur, “Librispeech: An asr corpus based on public domain audio books,” in *IEEE International Conference on Acoustics, Speech and Signal Processing (ICASSP)*, Brisbane, Australia, Apr. 2015, pp. 5206–5210.
- [45] G. Tzanetakis and P. Cook, “Musical genre classification of audio signals,” *IEEE Transactions on Speech and Audio Processing*, vol. 10, no. 5, pp. 293–302, 2002.
- [46] B. L. Sturm, “An analysis of the GTZAN music genre dataset,” in *International ACM Workshop on Music Information Retrieval with User-Centered and Multimodal Strategies*, Nara, Japan, Oct. 2012.
- [47] “LibriVox: Free public domain audiobooks,” <https://librivox.org>, accessed: 2023-03-27.
- [48] D. Kingma and J. Ba, “ADAM: A method for stochastic optimization,” 2014, arXiv:1412.6980.
- [49] ITU-T Recommendation P.862.2, “Wideband extension to recommendation P.862 for the assessment of wideband telephone networks and speech codecs,” ITU, Recommendation, Nov. 2007.
- [50] A. Briegleb, T. Haubner, V. Belagiannis, and W. Kellermann, “Localizing spatial information in neural spatiospectral filters,” 2023, arXiv:2303.08052.
- [51] F. Pedregosa, G. Varoquaux, A. Gramfort, V. Michel, B. Thirion, O. Grisel, M. Blondel, P. Prettenhofer, R. Weiss, V. Dubourg, J. Vanderplas, A. Passos, D. Cournapeau, M. Brucher, M. Perrot, and E. Duchesnay, “Scikit-learn: Machine learning in Python,” *Journal of Machine Learning Research*, vol. 12, pp. 2825–2830, 2011.